Symmetry breaking for semiconductor photocatalysis

Jun Di[1,2], Wei Jiang[1,*], Zheng Liu[2,*]

[1] School of Chemistry and Chemical Engineering, National Special Superfine Powder Engineering Research Center, Nanjing University of Science and Technology, Nanjing, 210094, China

[2] School of Materials Science & Engineering, Nanyang Technological University, Singapore 639798, Singapore

*Corresponding authors: superfine_jw@126.com; z.liu@ntu.edu.sg

Abstract

Numerous strategies have been developed to tailor the photocatalytic performance of catalysts. However, any essential general regularity exists in these strategies for activity improvement? It is desirable to explore the general regularity in these strategies, thus guiding further developments in the field of photocatalysis. In this review, we proposed that the key or essential nature of improved photocatalytic activity depends considerably on the symmetry breaking of the materials. The detailed contributions of symmetry breaking to the increased photocatalytic activity have been intensely discussed and summarized based on the location of symmetry breaking, namely, spontaneous symmetry breaking in the material interior, localized symmetry breaking on the material surface, and external fields induced symmetry breaking beyond the materials.

Fundamental in photocatalysis

Many means have been adopted to deal with the energy shortage and environmental issues, among which artificial photocatalysis under ambient conditions provides a promising alternative solution. With the appropriate photocatalysts as

intermedium and solar light as the driving force, many chemical reactions can be triggered sustainably to solve these issues, such as CO_2 photoreduction to yield solar fuels and valuable chemicals, water splitting to yield H_2 and O_2, N_2 photoreduction to yield NH_3 as well as photodegradation and mineralization of water pollutants.[1-10] During the photocatalysis process, the semiconductor is been excited to produce electron-hole pairs under solar light irradiation. The formed charge carriers will then migrate from bulk to material surface and arrive the surface's active sites. During the carrier migration and transfer process, it will suffer from recombination and lots of charge carriers are lost before involve in the catalysis reaction. Finally, the surface-arrived carriers will trigger corresponding interfacial redox catalytic reactions. Since the relatively low performance, a sizeable margin still exists for scale applications of photocatalysis. One of the core issues in photocatalysis should be improving the catalytic activity.

Up to now, many different strategies show huge potential to tailor photocatalytic performance of catalysts, such as doping, defect engineering, surface modification and so on (**Table S1**).[11-18] A question naturally arises: why these strategies can boost the photocatalytic activity? Any essential general regularity of these strategies behind activity improvement? It is desirable to explore the general regularity in these strategies, thus guiding further developments in the field of photocatalysis. According to a summary of the literatures, we found the key or essential nature of improved photocatalytic activity actually depends considerably on the symmetry breaking of the materials.

Charge separation and transfer is a highly complicated process in photocatalysis reaction. The generation of charge carriers is at femtoseconds level, transfer of charge carriers requires hundreds of picoseconds, and interfacial catalytic reaction time to consume charge carriers needs several nanoseconds to microseconds.[19, 20] Comparatively, charge recombination is among the time dimension of several picoseconds to tens of nanoseconds. Thus, the majority of generated charge carriers will be lost via recombination during the migration and interfacial catalytic reaction process. Fortunately, the charge separation efficiency can be increased by the symmetry

breaking of materials. Specifically, local polarization will appear once the existence of structure difference by symmetry breaking. Since the polarization can form directional electric field, the directional migration of electrons or holes can be accelerated, thus the separation efficiency of photogenerated electron-hole pairs can be improved. Depending on the location of the asymmetric states in the material (**Figure 1**), different strategies are divided into three categories: spontaneous symmetry breaking in the material interior, localized symmetry breaking on the material surface, and external fields induced symmetry breaking beyond the materials.

Spontaneous symmetry breaking in material interior

To improve the photocatalytic activity, numerous strategies have been developed, such as heteroatom doping, vacancy creation, disorder control and so on.[21-34] All these strategies shared a feature that partial atomic configuration in materials undergoes variety, no matter the atomic types, contents, locations or others, to decrease the symmetry of material interior.

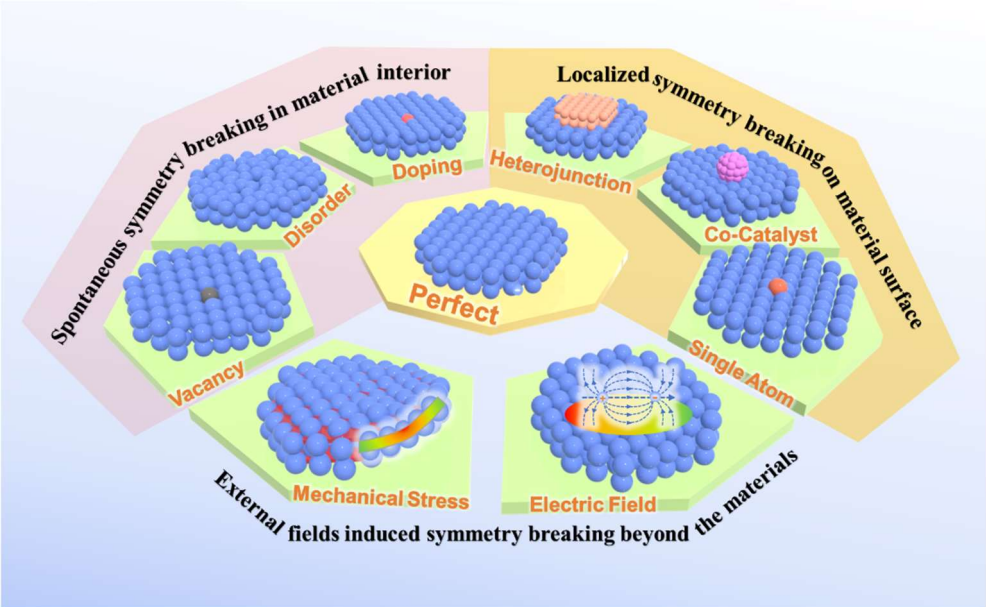

Figure 1. Schematic illustration of different strategies to break the local symmetry of materials.

As a common strategy to optimize traditional photocatalysts, heteroatoms doping

can build intermediate states or change the electronic structure, providing opportunities to tailor the photocatalytic activity. Apart from building an additional band between the intrinsic conduction band (CB) and valence band (VB), the efficacious doping usually can be used as trapping states to accelerate photogenerated charge carrier separation.[35] For instance, by doping O into $ZnIn_2S_4$ nanosheets via S site replacing, the local electronic structure and electric field intensity can be adjusted.[21] As proved by the ultrafast transient absorption (TA) spectroscopy, this symmetry breaking in $ZnIn_2S_4$ nanosheets leads to a 1.53 times improved average recovery lifetime of photoexcited electrons, enabling 4.5 times higher photocatalytic hydrogen evolution activity. In another case, C doping is employed to tailor the charge distribution inside the Bi_3O_4Cl materials (**Figure 2a**).[19] The electrostatic potential differences (ΔE) between [Bi_3O_4] and doped [Cl] slices are determined by density functional theory calculation. The C-Bi_3O_4Cl exhibits a ΔE value of 7.36 eV, much higher than those of P (3.97 eV), S (4.15 eV), N (5.12 eV), B (4.26 eV), F (4.52 eV), and Br (4.93 eV) doped counterparts, suggesting the C doping is a favorable alternative to maximize break the symmetry. Owing to the intensified nonuniform charge distribution, 126-fold increased internal electric field intensity can be obtained in C-Bi_3O_4Cl relative to Bi_3O_4Cl, enabling the greatly increased photocatalytic water oxidation activity.

Apart from nonmetal element doping, the metal doping methods may show a stronger effect in regulating the electronic structure and carrier dynamics. The doping of $Cu^{\delta+}$ into ZnAl-LDH nanosheets has been demonstrated to be able to boost the photocatalytic N_2 reduction activity.[24] This coordinatively unsaturated $Cu^{\delta+}$ ($\delta < 2$) with electron-rich property contributed to the separation of photogenerated charge carriers, resulting in 6.4 times higher NH_3 formation rate. Further study found that doping Mo into $W_{18}O_{49}$ nanowires can polarize the adsorbed N_2 molecules and facilitate electron transfer from coordinatively unsaturated sites to N_2, making N≡N more feasible for dissociation via proton coupling.[22] A 7-fold higher NH_3 generation rate can thus be obtained over Mo-$W_{18}O_{49}$ relative to $W_{18}O_{49}$ through N_2 photoreduction. These results certainly demonstrate that element doping is an efficacious tool to break the material symmetry, then tailor the carrier dynamics and further increase the

photocatalytic behavior.

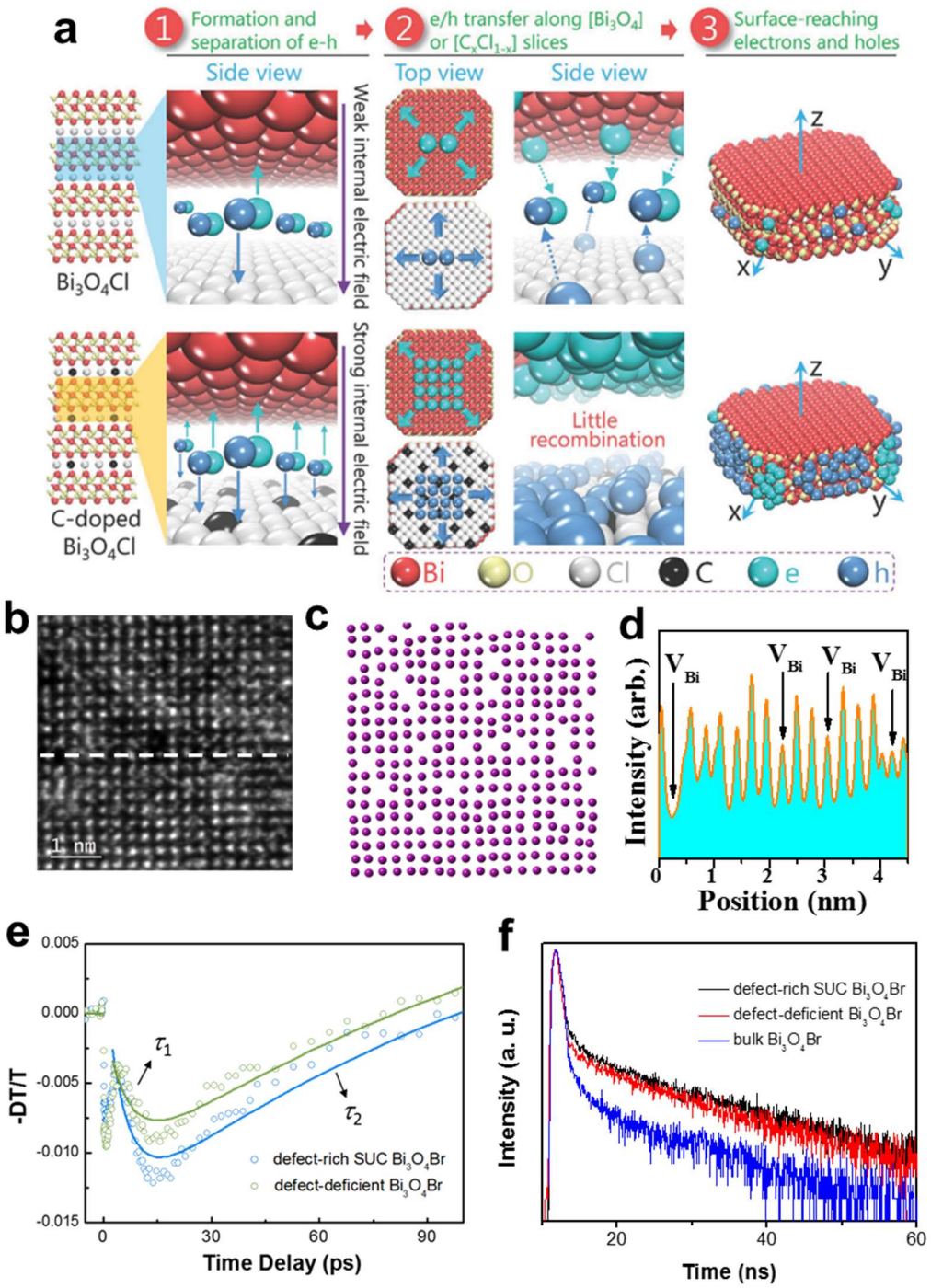

Figure 2. **Charge separation process in C-doped Bi_3O_4Cl and defect-rich Bi_3O_4Br.** (a) Schematic illustration of the separation and migration of electrons and holes in the bulk of the pure and C-doped Bi_3O_4Cl. Image reproduced with permission from [19]. (b) STEM image, (c) structural model and (d) line profiles of defect-rich Bi_3O_4Br. (e) Ultrafast TA spectroscopy and (f) time-resolved transient PL decay of Bi_3O_4Br

materials. Image reproduced with permission from [29].

In addition to doping, vacancy creation is an appealing strategy to destroy material interior structure. As such, the local symmetry of materials decreases and forms local polarization. Taking the widespread O vacancy as an example, the loss of oxygen atoms will endow an electron-rich state around O vacancy. Then a local electric field can be established for charge migration to catalytic sites.[36] Benefiting from the O vacancy for boosting charge separation, the CO formation rate over $BiOIO_3$ can be improved from 5.76 to 17.33 μmol g^{-1} h^{-1}. In another case, the O vacancies are engineered into BiOBr atomic layers via ultraviolet light irradiation process.[26] As proved by the fluorescence emission decay spectra, the engineered O vacancies increase the carrier lifetime from 1.65 to 3.12 ns over BiOBr atomic layers, further resulting in 20 times higher CO_2 photoreduction activity to yield CO (87.4 μmol g^{-1} h^{-1}). Our group employed a surface recrystallization strategy to tune the vacancy concentrations in Bi_3O_4Br atomic layer (**Figure 2b-f**).[29] It is proved that the generation of oxygen vacancies in Bi_3O_4Br is directly related to the absence of bismuth atoms in the material. The defects can tune the local atomic arrangement and electronic structure, while serving as surface charge separation centers to promote the separation of charge carriers, thus improving the photocatalytic hydrogen production and nitrogen fixation efficiency.

It is worth noting that there is an optimal value for symmetry breaking. For example, the defect content is not as high as possible. Our work found the Se vacancies in $PtSe_2$ favor the exposure of isolated Pt atoms and can improve the hydrogen evolution activity.[34] If only from the point of view of the active site, it should be that more defects can afford more Pt active sites and can offer more access for charge carriers to involve in the interfacial redox reactions, leading to better performance. That is, almost every Pt atom is isolated should show the best performance. However, it can be found that the $PtSe_x$ ($1.2 < x < 1.3$) shows the best performance. Partial Se vacancies lead to a decrease in symmetry, while too many Se vacancies will opposite lead to increased symmetry.

The local polarization generated after symmetry breaking not only affects the

behavior of electrons, but also affects the behavior of molecules on the surface of the material (coordination mode, coordination number, etc.). Moreover, it may even change the mode of interaction force towards intermediate state[37] or adjust the entire reaction pathway of the molecules,[38] such as C-C coupling, etc.[39-41] Our group demonstrated the Bi-O vacancy pairs in $Bi_{24}O_{31}Br_{10}$ can create local polarization field to facilitate charge migration from $Bi_{24}O_{31}Br_{10}$ to vacancy pairs.[37] Moreover, symmetry broken defective surface shows stronger non-covalent interaction with CO* intermediate than perfect surface during CO_2 photoreduction process (**Figure 3a-c**), resulting in the variety of rate-limiting step from CO* formation over perfect surface to COOH* formation over Bi-O vacancy pairs tuned surface. After incorporating isolated Cu atoms into $Bi_{24}O_{31}Br_{10}$ atomic layers by replacing Bi atoms, polarized Cu-Bi site pairs can be created.[42] It can improve the non-covalent interaction between the material's surface and N_2 molecules, then weaken the covalent bond order in N-N. The hydrogenation mode can be tuned from associative distal pathway over $Bi_{24}O_{31}Br_{10}$ to alternating pathway over Cu-$Bi_{24}O_{31}Br_{10}$.

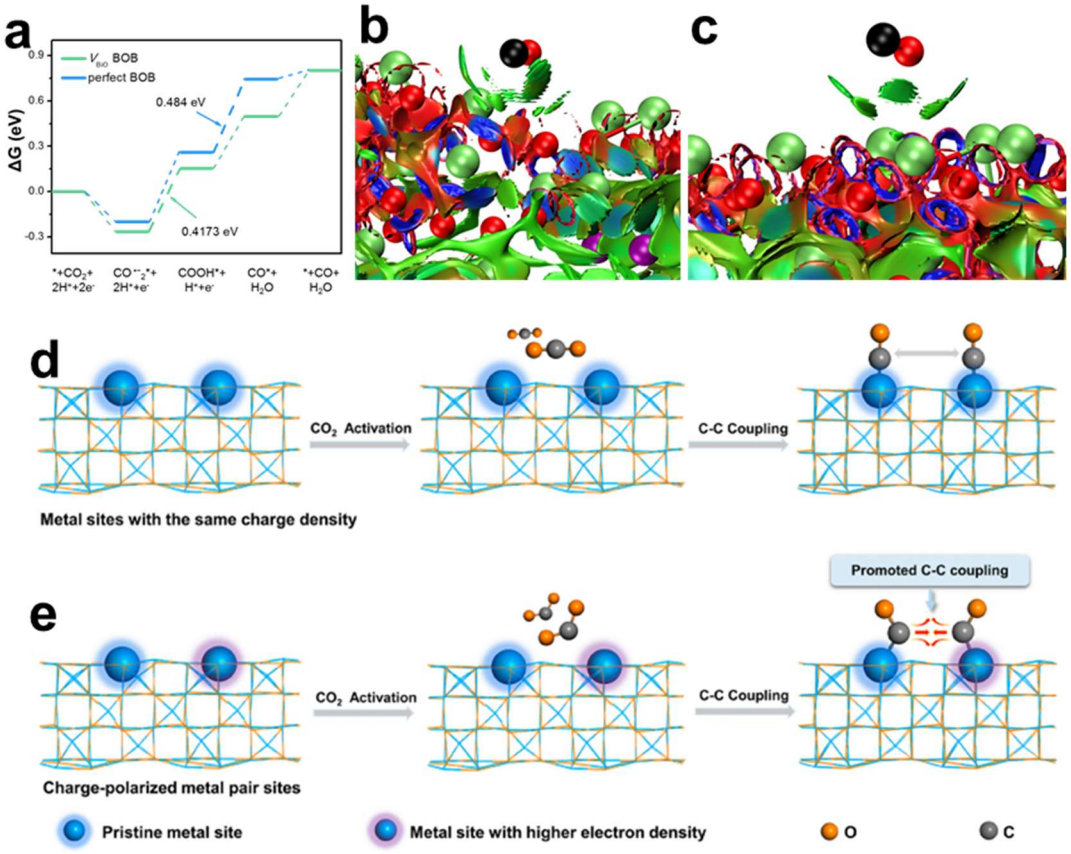

Figure 3. **Reaction intermediate and processes**. (a) Calculated free-energy diagram for CO_2 reduction to CO on the V_{BiO}-BOB and perfect BOB. Gradient isosurfaces for non-covalent interaction between CO* intermediate and (b) V_{BiO} sites, and (c) perfect surface. Image reproduced with permission from [37]. Scheme of the C-C coupling process over (d) conventional metal-based photocatalyst, and (e) charge-polarized metal pair sites on the metal-based photocatalyst. Image reproduced with permission from [40].

Through the symmetry breaking design, charge-polarized metal pair sites can be further created to trigger C-C coupling.[41] The core rely on the material design of asymmetric state. For instance, Sun et al. designed charge-polarized Co-Co pair sites in Co_3O_4 via O vacancy engineering (**Figure 3d, e**).[40] Due to the abundant O vacancies in partially reduced Co_3O_4 nanosheets, the Co sites surrounding the vacancies own higher Bader charge relative to other Co sites, resulting in the formation of asymmetric charge distributed Co-Co pair sites. This configuration can lower the energy barrier and accelerate the coupling of asymmetric COOH* intermediates, leading to the highly selective CO_2-to-CH_3COOH conversion. The optimized CH_3COOH generation rate reaches 2.95 μmol g^{-1} h^{-1} in simulated air with 92.5% selectivity and 2.75% conversion. In another case, building S vacancies in $AgInP_2S_6$ atomic layers can form electron-rich Ag atoms near the S vacancies, which favors the capture of *CO molecules.[39] Due to the abundant key reaction intermediates on the surface, the energy barrier of C-C coupling can thus be lowered, resulting in higher selectivity to yield C_2H_4. The S vacancies tuned $AgInP_2S_6$ atomic layers shows a C_2H_4 formation rate of 44.3 μmol g^{-1} in first hour and the yield-based selectivity arriving ~73 %. Further study found the asymmetric $Metal_1$-$Metal_2$ atom sites facilitate the C-C coupling and the existed O vacancy can reduce energy barriers in hydrogenation step and further promote C-C coupling reaction.[41] Due to the distinct charge distributions of neighboring C_1 intermediates induced by asymmetric Zn-Ge site pairs, the C-C coupling process of C_1 intermediates is promoted. As a result, the CH_3COOH generation rate via CO_2 photoreduction reaches 12.7 μmol g^{-1} h^{-1} and selectivity of 66.9%. Generally, symmetry

breaking in the materials to create asymmetric charge distributed state will not only exhibit enhanced photocatalytic properties of the host materials, but also induce new reactions like C-C coupling.

Localized symmetry breaking on material surface

Additional surface tuning on the materials can also partially break the symmetry of materials, such as single atom engineering, surface functionalization, co-catalysts modification, heterojunction, heterophase junction, homojunction and so on.[43-52] Single atom loading can generate localized electric field effects on the surfaces, adjusting the charge carrier migration process. When acting on chemical reaction, the reaction substrate will have a localized high concentration distribution around the tip structure, which is expected to accelerate the kinetic process of chemical reaction. For instance, our previous work engineered Co single atoms into Bi_3O_4Br atomic layers for CO_2 photoreduction (**Figure 4a-f**).[53] The single-atom Co as a localized charge separation center greatly prolongs the photogenerated carrier lifetime of the material, as certified by ultrafast TA spectra. The optimized Co-Bi_3O_4Br material exhibits excellent photocatalytic performance to yield CO, with a rate of 107.1 μmol g^{-1} h^{-1} in pure water. Furthermore, the introduction of Co single atoms can reduce the CO_2 activation energy and change the rate-determining step of the reaction. The rate-determining step on the surface of Bi_3O_4Br material is the formation of COOH*, while it changes to CO* desorption on the surface of Co-Bi_3O_4Br.

The surface halogenation strategy has been demonstrated as an effective surface polarization protocol to boost CO_2 photoreduction. The Br ions are anchored on the Bi atoms of $Bi_2O_2(OH)(NO_3)$ (BON) by replacing surface hydroxyls. As proved by femtosecond ultrafast TA spectroscopy and charge difference calculation, this surface polarization leads to the fast charge separation and substantially prolonged lifetime (**Figure 4g-i**).[54] The Br-BON materials show 73 times improved photocatalytic activity to yield CO, with the formation rate of 8.12 μmol g^{-1} h^{-1}. Similar surface polarization can also be realized via surface I-grafting in $Bi_4Ti_3O_{12}$, which contributed to 6 times increased CO_2 photoreduction efficiency of $Bi_4Ti_3O_{12}$ to yield CO.[55]

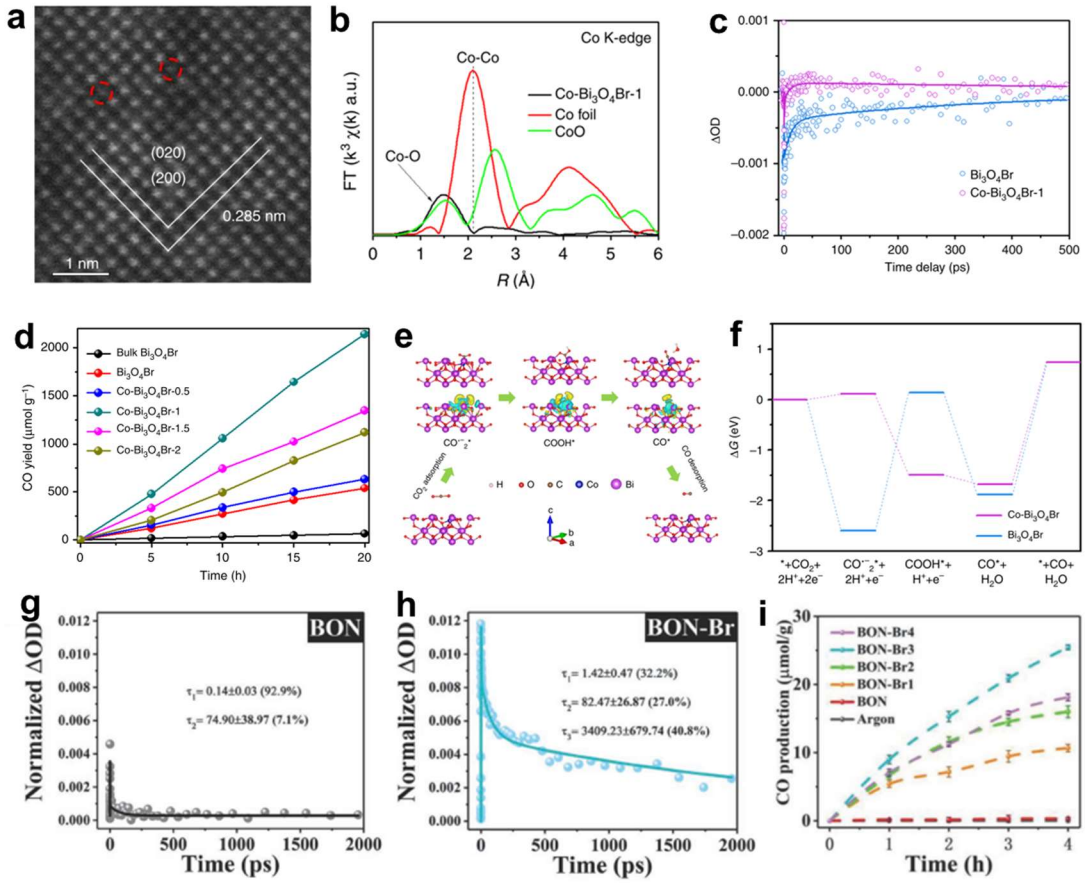

Figure 4. **Photocatalytic CO_2 reduction of Co-Bi_3O_4Br and BON-Br**. (a) STEM image, (b) EXAFS Co K-edge spectra of Co-Bi_3O_4Br-1, (c) ultrafast TA spectra of Bi_3O_4Br and Co-Bi_3O_4Br, (d) CO_2 photoreduction performance, (e) schematic representation of CO_2 photoreduction mechanism on the Co-Bi_3O_4Br, (f) free energy diagrams of CO_2 photoreduction to CO. Image reproduced with permission from [53]. Femtosecond ultrafast TA spectroscopy of (g) BON and (h) BON-Br, (i) time-dependence CO yields over BON-Br. Image reproduced with permission from [54].

Engineering specific co-catalysts onto the host catalysts is a common means to optimize the photocatalytic performance. One of the main roles is creating interfaces with differentiated work functions, thus leading to the interfacial polarized electric field. Take the graphdiyne (GDY) co-catalyst as an example, Yu et al. demonstrated the delocalized electrons in GDY can hybrid with the empty orbitals in TiO_2 within the TiO_2/GDY materials, resulting in the creation of internal electric field at interfaces.[56] Due to the symmetry of TiO_2 surface being destroyed by the GDY modification, the

local polarization will happen to boost the charge migration, then account for the improved photocatalytic CO_2 reduction performance. Similar process can also be found in our CoN_2/BiOBr system by using CoN_2 as cocatalyst (**Figure 5a-c**).[57] Interfacial potential difference leads to the transfer of electrons from BiOBr to CoN_2, thus improving the photocatalytic CO_2 reduction activity of BiOBr for roughly 6 times, with the CO formation rate of 67.8 μmol g^{-1} h^{-1}. This localized interface symmetry breaking in co-catalysts modified materials has undoubtedly been proved as one of the important factors in enhancing catalytic performance.

Similarly, the heterojunction or heterophase junction also shows interfacial texture difference, then interfacial polarization will happen to boost interfacial charge separation.[58, 59] Zhu et al. constructed interfacial electric field through dual-porphyrin coupling.[60] It is formed via the π–π stacking interaction between tetrakis (4-carboxyphenyl) zinc porphyrin (ZnTCPP) and tetrakis (4-hydroxy-phenyl) porphyrin (THPP). Due to the differentiated work functions, the interfacial electric field is created directed from ZnTCPP to THPP, enabling rapid transfer of photogenerated electrons and then realizing higher photocatalytic H_2 evolution rate. Wu's group designed ZnSe/CdS heterojunction by anchoring ZnSe quantum dots (QDs) on CdS rods.[61] This surface-anchored ZnSe QDs favors ultrafast (≈2 ps) electron and hole separation, as proved by ultrafast TA spectroscopy. Furthermore, the surface photovoltage spectroscopy offers a direct image of spatially separated electrons in CdS and holes in ZnSe due to the formed interfacial electric field. Therefore, a higher photocatalytic CO_2-CO conversion rate is achieved over ZnSe/CdS (11.3 μmol g^{-1} h^{-1}), nearly 2 times higher than CdS. In another case, WO_3/CdS heterojunction with significantly different atomic structures are designed (**Figure 5d-i**).[62] The electron transfer and migration by the internal electric field at the interface can be determined by ultrafast TA spectroscopy. Moreover, the interfacial charge redistribution phenomenon can be observed through surface potential imaging due to the charge migration, enabling selective accumulation of electrons and holes in CdS and WO_3, respectively. As a consequence, the NH_4^+ production rate can be improved from 7.2 μmol g^{-1} h^{-1} over CdS to 35.8 μmol g^{-1} h^{-1} over WO_3/CdS.

Generally, the construction of heterojunction creates the differentiated interfacial components and thus the interfacial symmetry is broken to form interfacial electric field. It is worth noting that the heterojunction usually has fewer interfaces due to the large material size, so the overall variety of the material through the symmetry breaking is relatively small. As a result, the activity improvement in many heterojunction systems is often limited, usually 2-5 times. Similar results can also be observed in heterophase junction. Moreover, there is an optimal ratio in heterojunction, higher content of guest component will lead to lower performance. This possibly resulted from the symmetry rising again. In contrast, the modification of atomically-thin materials is easier to significantly improve the photocatalytic activity,[63, 64] which may also be related to easily and largely symmetry breaking of 2D matrix.

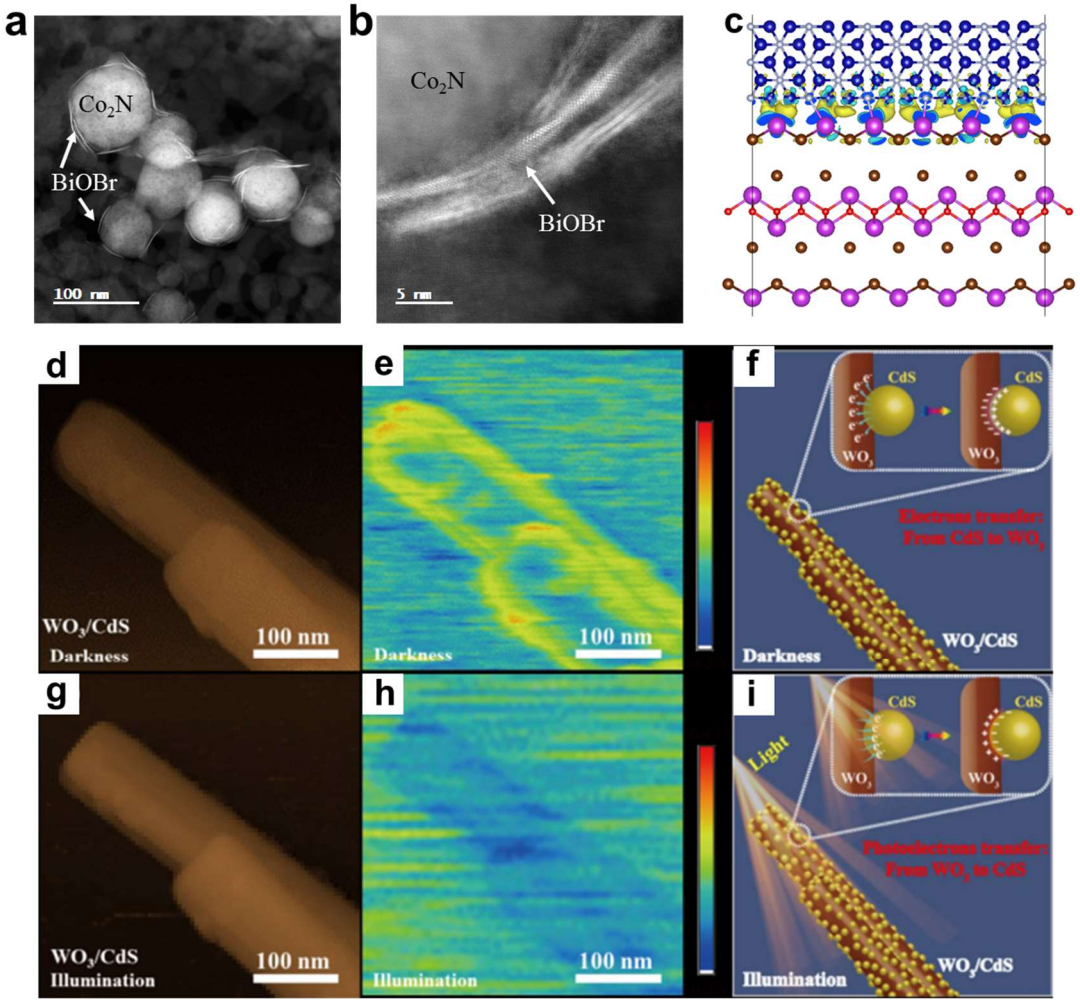

Figure 5. **Charge migration process in CoN_2/BiOBr and WO_3/CdS**. (a, b) STEM images of CoN_2/BiOBr, (c) charge difference of Co_2N/BiOBr interface. Image

reproduced with permission from [57]. (d) AFM image and (e) corresponding surface potential of WO_3/CdS heterojunction in darkness, and (f) the diagram of electron transfer direction from CdS to WO_3 in darkness. (g) AFM image and (h) corresponding surface potential of WO_3/CdS heterojunction under illumination, and (i) the diagram of photoelectron transfer direction from WO_3 to CdS under illumination. Image reproduced with permission from [62].

External fields induced symmetry breaking beyond the materials

In addition to the material itself, symmetry breaking can also be realized by external fields such as microwaves, mechanical stress, temperature gradient, electric field, magnetic field, to boost photocatalytic reactions.[65] For instance, ultrasonic is employed as mechanical stress to boost the photocatalytic H_2 evolution performance of g-C_3N_4 (**Figure 6a-c**).[66] The additive dipole moment of polar tri-s-triazine units contributed to the in-plane polarization enhancement, resulting in better photocatalytic activity of g-C_3N_4 nanosheets. Huang et al. demonstrated the existence of strong ferroelectric spontaneous polarization along [100] direction of $SrBi_4Ti_4O_{15}$ nanosheets, thus efficient bulk charge separation along opposite direction can be acquired.[67] In another case, corona poling is employed to strengthen the ferroelectric polarization of Bi_3TiNbO_9 nanosheets, so as to boost bulk charge separation.[68] As proved by COMSOL simulations, after imposing a poling voltage, domains tend to gradually switch to be aligned and result in a polarization-induced electric field (**Figure 6d-f**). This electric field is beneficial to the separation of charge carriers and enables ~5 times increased CO_2 photoreduction activity (**Figure 6g-i**). Similar corona poling process to boost the ferroelectric polarization is also realized over $Bi_4Ti_3O_{12}$.[55] This corona poling induced enhanced bulk charge separation make the CO production rate improved from 1.7 to 5.2 μmol g^{-1} h^{-1} over $Bi_4Ti_3O_{12}$. Apart from these, other external fields are also desirable to adjust the symmetry inside the materials and further increase the photocatalytic activity.

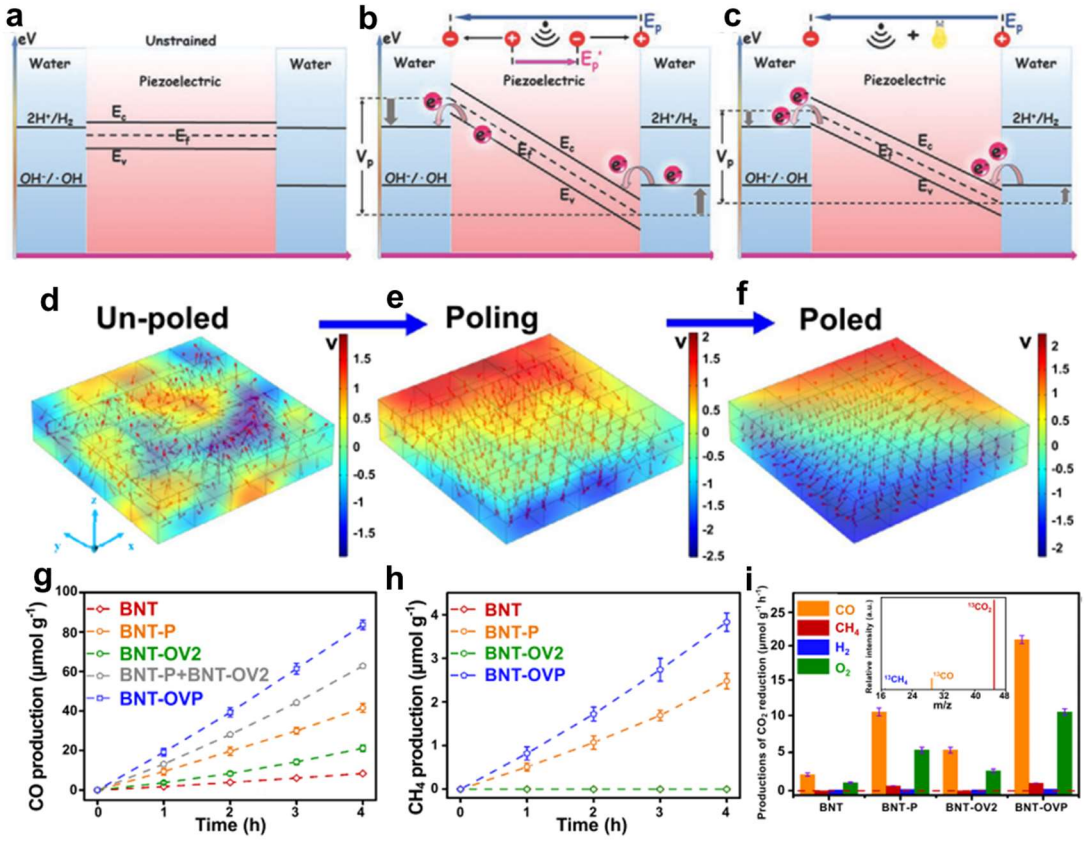

Figure 6. **CO_2 photoreduction reaction over Bi_3NbTiO_9**. (a-c) Schematic mechanism of the photo-improved piezocatalytic process. Image reproduced with permission from [66]. COMSOL simulation of polarization-induced electric field on Bi_3NbTiO_9 sheets: (d) un-poled, (e) intermediate poled, (f) fully poled. (g, h) CO and CH_4 production curves and (i) corresponding evolution rates of CO, CH_4, and H_2 over Bi_3NbTiO_9 materials. Image reproduced with permission from [68].

Concluding remarks

Considerable progress has been made in boosting photocatalytic activity via various tactics. We proposed that the key or essential nature behind the enhanced activity is highly related to the material symmetry breaking. Based on the location difference, various optimization strategies have been classified into three types: symmetry breaking in material interior, symmetry breaking on material surface and symmetry breaking beyond the materials, as well as the relevant mechanism of action and structure-activity relationship have been surveyed. Despite some progresses, the research on symmetry breaking design for photocatalytic behavior improvement is still

at its infancy stage. The quantification of symmetry breaking in materials should be a logical step forward, help to precise correlate the catalytic performance with its asymmetry degree. Furthermore, theoretical work regarding symmetry breaking for mechanistic understanding is still inadequate. More efforts should be committed to optimize calculation conditions with closer to realistic reaction systems, thus achieving a deeper understanding. In addition to directly solar irradiation, external field such as thermal field, electric field or photovoltaic device can be integrated to build suitable photocatalytic devices. Bearing these features in mind, further reasonable design strategies are desirable to be developed to make a historic breakthrough in photocatalytic performance.

Acknowledgements

This work was supported by Singapore Ministry of Education AcRF Tier 2 (MOE2019-T2-2-105), AcRF Tier 1 RG4/17, RG161/19, Fundamental Research Funds for the Central Universities (Project 30922010302) and Start-Up Grant from Nanjing University of Science and Technology (Project AE89991/397).

Declaration of interests

The authors declare no interests.

References

1. Takata T. *et al.* (2020) Photocatalytic water splitting with a quantum efficiency of almost unity. *Nature* 581, 411-414.
2. Jiang Z. *et al.* (2020) Filling metal–organic framework mesopores with TiO_2 for CO_2 photoreduction. *Nature* 586, 549-554.
3. Kranz C. *et al.* (2021) Characterizing photocatalysts for water splitting: from atoms to bulk and from slow to ultrafast processes. *Chem. Soc. Rev.* 50, 1407-1437.
4. Feng X.Z. *et al.* (2022) Unlocking bimetallic active sites via a desalination strategy for photocatalytic reduction of atmospheric carbon dioxide. *Nat. Commun.* 13, 2146.
5. Zhao D.M. *et al.* (2021) Boron-doped nitrogen-deficient carbon nitride-based Z-scheme heterostructures for photocatalytic overall water splitting. *Nat. Energy* 6, 388-397.
6. Lin L.H. *et al.* (2020) Molecular-level insights on the reactive facet of carbon nitride single crystals photocatalysing overall water splitting. *Nat. Catal.* 3, 649-655.

7. Jiang, X.Y. *et al.* (2022) Plasmonic active "hot spots"-confined photocatalytic CO_2 reduction with high selectivity for CH_4 production. *Adv. Mater.* 34, 2109330.
8. Liao L.L. *et al.* (2022) Highly reductive photocatalytic systems in organic synthesis. *Trends Chem.* 4, 512-527.
9. Lin L.H. *et al.* (2020) Visible-light-driven photocatalytic water splitting: Recent progress and challenges. *Trends Chem.* 2, 813-824.
10. Chen F. *et al.* (2022) Single-atom iron anchored tubular g-C_3N_4 catalysts for ultrafast Fenton-like reaction: roles of high-valent iron-oxo species and organic radicals. *Adv. Mater.* 34, 2202891.
11. Li J. *et al.* (2021) Interfacial engineering of $Bi_{19}Br_3S_{27}$ nanowires promotes metallic photocatalytic CO_2 reduction activity under near-infrared light irradiation. *J. Am. Chem. Soc.* 143, 6551-6559.
12. Han Q.T. *et al.* (2021) Hollow $InVO_4$ nanocuboid assemblies toward promoting photocatalytic N_2 conversion performance. *Adv. Mater.* 33, 2006780.
13. Zhang Y.T. *et al.* (2021) Two-dimensional defective boron-doped niobic acid nanosheets for robust nitrogen photofixation. *ACS Nano* 15, 17820-17830.
14. Liao G.F. *et al.* (2022) Emerging frontiers of Z-scheme photocatalytic systems. *Trends Chem.* 4, 111-127.
15. Zhou P. *et al.* (2021) Single-atom Pt-I_3 sites on all-inorganic Cs_2SnI_6 perovskite for efficient photocatalytic hydrogen production. *Nat. Commun.* 12, 4412.
16. Cheng C. *et al.* (2021) An inorganic/organic S-scheme heterojunction H_2-production photocatalyst and its charge transfer mechanism. *Adv. Mater.* 33, 2100317.
17. Kou M.P. *et al.* (2022) Molecularly engineered covalent organic frameworks for hydrogen peroxide photosynthesis. *Angew. Chem. Int. Ed.* 61, e202200413.
18. Li J.Y. *et al.* (2022) Subnanometric alkaline-earth oxide clusters for sustainable nitrate to ammonia photosynthesis. *Nat. Commun.* 13, 1098.
19. Li J. *et al.* (2016) Giant enhancement of internal electric field boosting bulk charge separation for photocatalysis. *Adv. Mater.* 28, 4059-4064.
20. Zhang L.Y. *et al.* (2022) Emerging S-scheme photocatalyst. *Adv. Mater.* 34, 2107668.
21. Yang W.L. *et al.* (2016) Enhanced photoexcited carrier separation in oxygen-doped $ZnIn_2S_4$ nanosheets for hydrogen evolution. *Angew. Chem. Int. Ed.* 55, 6716-6720
22. Zhang N. *et al.* (2018) Refining defect states in $W_{18}O_{49}$ by Mo doping: a strategy for tuning N_2 activation towards solar-driven nitrogen fixation. *J. Am. Chem. Soc.* 140, 9434-9443
23. Lei F.C. *et al.* (2015) Atomic-layer-confined doping for atomic-level insights into visible-light water splitting. *Angew. Chem. Int. Ed.* 54, 9266-9270
24. Zhang S. *et al.* (2020) Efficient photocatalytic nitrogen fixation over $Cu^{\delta+}$-modified defective ZnAl-layered double hydroxide nanosheets. *Adv. Energy Mater.* 10, 1901973
25. Zu X.L. *et al.* (2021) Ultrastable and efficient visible-light-driven CO_2 reduction triggered by regenerative oxygen-vacancies in $Bi_2O_2CO_3$ nanosheets. *Angew. Chem. Int. Ed.* 60, 13840-13846
26. Wu J. *et al.* (2018) Efficient visible-light-driven CO_2 reduction mediated by defect-engineered BiOBr atomic layers. *Angew. Chem. Int. Ed.* 57, 8719-8723

27. Chen S.C. *et al.* (2019) Oxygen vacancy associated single-electron transfer for photofixation of CO_2 to long-chain chemicals. *Nat. Commun.* 10, 788
28. Zhao Y.X. *et al*. (2019) Tuning oxygen vacancies in ultrathin TiO_2 nanosheets to boost photocatalytic nitrogen fixation up to 700 nm. *Adv. Mater.* 31, 1806482
29. Di J. *et al*. (2019) Defect-tailoring mediated electron–hole separation in single-unit-cell Bi_3O_4Br nanosheets for boosting photocatalytic hydrogen evolution and nitrogen fixation. *Adv. Mater.* 31, 1807576
30. Wang L. *et al*. (2021) Bismuth vacancy-induced efficient CO_2 photoreduction in BiOCl directly from natural air: a progressive step toward nature photosynthesis. *Nano Lett.* 21, 10260-10266
31. Dong X.A. *et al*. (2022) Insights into dynamic surface bromide sites in $Bi_4O_5Br_2$ for sustainable N_2 photofixation. *Angew. Chem. Int. Ed.* 61, e202200937
32. Shi Y.B. *et al*. (2021) Van der waals gap-rich BiOCl atomic layers realizing efficient, pure-water CO_2-to-CO photocatalysis. *Nat. Commun.* 12, 5923
33. Shi Y.B. *et al*. (2021) Simultaneous manipulation of bulk excitons and surface defects for ultrastable and highly selective CO_2 photoreduction. *Adv. Mater.* 33, 2100143
34. He Y.M. *et al*. (2022) Amorphizing noble metal chalcogenide catalysts at the single-layer limit towards hydrogen production. *Nat. Catal.* 5, 212-221
35. Sun X.D. *et al*. (2020) Thin-layered photocatalysts. *Adv. Funct. Mater.* 30, 1910005
36. Chen F. *et al*. (2020) Macroscopic spontaneous polarization and surface oxygen vacancies collaboratively boosting CO_2 photoreduction on $BiOIO_3$ single crystals. *Adv. Mater.* 32, 1908350
37. Di J. *et al*. (2021) Surface local polarization induced by bismuth-oxygen vacancy pairs tuning non-covalent interaction for CO_2 photoreduction. *Adv. Energy Mater.* 11, 2102389
38. Li X.D. *et al*. (2019) Selective visible-light-driven photocatalytic CO_2 reduction to CH_4 mediated by atomically thin $CuIn_5S_8$ layers. *Nat. Energy* 4, 690-699
39. Gao W. *et al*. (2021) Vacancy-defect modulated pathway of photoreduction of CO_2 on single atomically thin $AgInP_2S_6$ sheets into olefiant gas. *Nat. Commun.* 12, 4747
40. Zhu S. *et al*. (2021) Selective CO_2 photoreduction into C_2 product enabled by charge-polarized metal pair sites. *Nano Lett.* 21, 2324-2331
41. Zhu J.C. *et al*. (2021) Asymmetric triple-atom sites confined in ternary oxide enabling selective CO_2 photothermal reduction to acetate. *J. Am. Chem. Soc.* 143, 18233-18241
42. Di J. *et al*. (2022) Polarized Cu-Bi site pairs for non-covalent to covalent interaction tuning toward N_2 photoreduction. *Adv. Mater.* 34, 2204959
43. Gao C. *et al*. (2020) Heterogeneous single-atom photocatalysts: fundamentals and applications. *Chem. Rev.* 120, 12175-12216
44. Li J. *et al*. (2020) Accelerated dinitrogen electroreduction to ammonia via interfacial polarization triggered by single-atom protrusions. *Chem* 6, 885-901
45. Meng A.Y. *et al*. (2019) Dual cocatalysts in TiO_2 photocatalysis. *Adv. Mater.* 31, 1807660
46. Li H.J. *et al*. (2015) State-of-the-art progress in diverse heterostructured

photocatalysts toward promoting photocatalytic performance. *Adv. Funct. Mater.* 25, 998-1013
47. Zhang J. *et al*. (2008) Importance of the relationship between surface phases and photocatalytic activity of TiO_2. *Angew. Chem. Int. Ed.* 47, 1766-1769
48. Li P. *et al*. (2015) Hexahedron prism-anchored octahedronal CeO_2: crystal facet-based homojunction promoting efficient solar fuel synthesis. *J. Am. Chem. Soc.* 137, 9547-9550
49. Wang M.M. *et al.* (2022) Ni–Co bimetallic hydroxide nanosheet arrays anchored on graphene for adsorption-induced enhanced photocatalytic CO_2 reduction. *Adv. Mater.* 34, 2202960
50. Jin X.X. *et al.* (2020) Electron configuration modulation of nickel single atoms for elevated photocatalytic hydrogen evolution. *Angew. Chem. Int. Ed.* 59, 6827-6831
51. Xin Z.K. *et al.* (2022) Reductive carbon–carbon coupling on metal sites regulates photocatalytic CO_2 reduction in water using ZnSe quantum dots. *Angew. Chem. Int. Ed.* 61, e202207222
52. Liu P.G. *et al.* (2022) Synergy between palladium single atoms and nanoparticles via hydrogen spillover for enhancing CO_2 photoreduction to CH_4. *Adv. Mater.* 34, 2200057
53. Di J. *et al*. (2019) Isolated single atom cobalt in Bi_3O_4Br atomic layers to trigger efficient CO_2 photoreduction. *Nat. Commun.* 10, 2840
54. Hao L. *et al*. (2019) Surface-halogenation-induced atomic-site activation and local charge separation for superb CO_2 photoreduction. *Adv. Mater.* 31, 1900546
55. Liu L.Z. *et al*. (2021) Synergistic polarization engineering on bulk and surface for boosting CO_2 photoreduction. *Angew. Chem. Int. Ed.* 60, 18303-18308
56. Xu F.Y. *et al*. (2019) Graphdiyne: a new photocatalytic CO_2 reduction cocatalyst. *Adv. Funct. Mater.* 29, 1904256
57. Di J. *et al*. (2021) Cobalt nitride as a novel cocatalyst to boost photocatalytic CO_2 reduction. *Nano Energy* 79, 105429
58. Yang J. *et al*. (2021) A full-spectrum porphyrin-fullerene D-A supramolecular photocatalyst with giant built-in electric field for efficient hydrogen production. *Adv. Mater.* 33, 2101026
59. Chen X.J. *et al*. (2021) Efficient photocatalytic overall water splitting induced by the giant internal electric field of a g-C_3N_4/rGO/PDIP Z-scheme heterojunction. *Adv. Mater.* 33, 2007479
60. Jing J.F. *et al*. (2022) Construction of interfacial electric field via dual-porphyrin heterostructure boosting photocatalytic hydrogen evolution. *Adv. Mater.* 34, 2106807
61. Xin Z. K. *et al*. (2022) Rational design of dot-on-rod nano-heterostructure for photocatalytic CO_2 reduction: pivotal role of hole transfer and utilization. *Adv. Mater.* 34, 2106662
62. Xia P.F. *et al*. (2022) Designing a redox heterojunction for photocatalytic "overall nitrogen fixation" under mild conditions. *Adv. Mater.* 34, 2200563
63. Di J. *et al*. (2018) Ultrathin 2D photocatalysts: electronic-structure tailoring, hybridization, and applications. *Adv. Mater.* 30, 1704548
64. Di J. *et al*. (2018) Ultrathin two-dimensional materials for photo- and

electrocatalytic hydrogen evolution. *Mater. Today* 21, 749-770
65. Hu C. *et al*. (2021) Photocatalysis enhanced by external fields. *Angew. Chem. Int. Ed.* 60, 16309-16328
66. Hu C. *et al*. (2021) Exceptional cocatalyst-free photo-enhanced piezocatalytic hydrogen evolution of carbon nitride nanosheets from strong in-plane polarization. *Adv. Mater.* 33, 2101751
67. Tu S.C. *et al*. (2019) Ferroelectric polarization promoted bulk charge separation for highly efficient CO_2 photoreduction of $SrBi_4Ti_4O_{15}$. *Nano Energy* 56, 840-850
68. Yu H.J. *et al*. (2021) Synergy of ferroelectric polarization and oxygen vacancy to promote CO_2 photoreduction, *Nat. Commun.* 12, 4594

Glossary

Carrier lifetime: the average lifetime of carriers before recombination.
Conduction band (CB): the energy band formed by free electrons.
Density functional theory: one of the most widely used theoretical calculation technologies.
Local polarization: a phenomenon in which polarization occurs under certain conditions, causing its nature to deviate from its original state.
Symmetry breaking: the degree of symmetry decreases in the original system with high symmetry.
Two-dimensional (2D) materials: materials in which electrons can move freely (planar motion) on the nanoscale in only two dimensions
Ultrafast transient absorption (TA) spectroscopy: one of the powerful tools to study carrier dynamics.
Vacancy pairs: the associates of multiple consecutive vacancies.
Valence band (VB): the energy band formed by valence electrons.
Work function: the minimum energy required to move an electron from the interior of a solid to its surface.